Nanosecond Dynamics of the R → T Transition in Hemoglobin: Ultraviolet Raman Studies

K. R. Rodgers and T. G. Spiro*

Pulse-probe transient Raman spectroscopy, with probe excitation at 230 nanometers, reveals changes in signals arising from tyrosine and tryptophan residues of the hemoglobin molecule as it moves from the relaxed (R) to the tense (T) state after photodeligation. Signals associated with intersubunit contacts in the T state develop in about 10 microseconds but are preceded by quite different signals, which reach maximum amplitude in about 50 nanoseconds. These signals involve the interior tryptophan residues that bridge the A and E helices by means of H bonds between the indole rings and serine or threonine side chains. Alterations of the H bond strengths, as a result of interhelix motions, can account for the signals. A model is proposed here in which loss of the ligand from the heme binding pocket is concerted with inward motion of the adjacent E helix; this motion, along with a complementary motion of the proximal F helix, transmits the energy associated with heme deligation to the subunit interfaces, leading to the T state rearrangement.

The hemoglobin (Hb) molecule offers a convenient experimental system for the study of conformational motions in proteins. Crystal structures of ligated and unligated forms of the protein reveal multiple differences at both tertiary and quaternary levels (*1*, *2*). These structures are associated with the high- and low-affinity states R and T, which account for the main features of cooperative ligand binding (*3*–*7*). The pathway between these states has been the object of much research, but a molecular-level description of the R-T interconversion has been elusive. Because of cooperativity, intermediate states have low populations at equilibrium and must be accessed through protein modification or by kinetic methods. When the carbon monoxide adduct, HbCO, is photolyzed, the CO molecules are released from the heme in a fraction of a picosecond (8, 9), providing an opportunity to monitor the relaxation of the protein from the R to the T state. This relaxation is accompanied by small changes in the heme optical absorbance, from which time constants of 0.05, 0.7, and 18 μs have been extracted (*10*).

We have used transient resonance Raman (RR) spectroscopy to obtain structural information about the relaxation pathway (*11*). Laser excitation at 230 nm provides resonance enhancement of vibrational Raman bands of tyrosine (Tyr) and tryptophan (Trp) side chains (*12*, *13*), which serve as monitors of the local environment. When static spectra for HbCO and deoxyHb are compared, the difference spectrum, shown at the top of Fig. 1, shows numerous features, which have been tentatively identified (*11*) as arising from the Tyrα42 and Trpβ37 residues. These residues form specific hydrogen bonds (H bonds) across the $\alpha_1\beta_2$ subunit interface in the T state, which are broken in the R state (*1*). The transient difference spectra, obtained by subtracting the HbCO spectrum from the spectrum of its photoproduct at variable pulse-probe time delays, show the same signals (*11*) growing at about 10 μs (Fig. 1) during the last phase (*10*) of the protein relaxation.

We now report a different set of signals at much earlier times, whose intensity reaches a maximum at ~50 ns (Fig. 1), on the same time scale as the first relaxation phase found in the transient absorption data (*10*). Intriguingly, almost the same difference spectrum can be generated by subtracting the static RR spectrum of fully ligated Co,Fe hybrid (*14*) Hb from that of the half-ligated hybrid. (These species are obtained, respectively, by ligation with O_2, which binds to both metals, and by CO, which binds only to Fe.) In the spectral comparison (Fig. 2), the difference spectrum is essentially the same for the two hybrids, obtained by replacing Fe by Co in either the α or the β chains. The substitution of Co for Fe destabilizes the T state, because in the absence of ligand the Co is displaced from the heme plane to a smaller extent than is Fe (*15*). Although the doubly ligated Co,Fe hybrids have been found to crystallize in the quaternary T structure (*16*), the thermodynamic data of Ackers and others (*7*) strongly indicate that the solution state is R. Likewise, the position of the Fe-His band in the visible excitation RR spectrum indicates that the doubly ligated hybrids are in the R state unless inositol hexaphosphate is added (*17*). (It is possible that the high salt concentration used for crystallization shifts the structure to T.) We interpret the Co,Fe difference spectra as reflecting tertiary changes within the R state that result from the loss of ligand from half of the chains. Likewise, the 50-ns difference spectrum for the native HbCO photoproduct must reflect tertiary changes induced by deligation, before the R-T conversion.

Significantly, however, the early difference spectrum is not formed immediately, but has a ~50-ns rise time, even though deligation occurs in less than a picosecond (8, 9). About half of the photodissociated CO molecules recombine geminately (*18*), and the time constant for this process is also ~50 ns (*10*, *19*). The rest of the CO escapes from the binding pocket and must do so on the same time scale. Consequently, we infer that the 50-ns RR difference spectrum reflects a tertiary change that accompanies emptying of the binding pocket, rather than deligation per se.

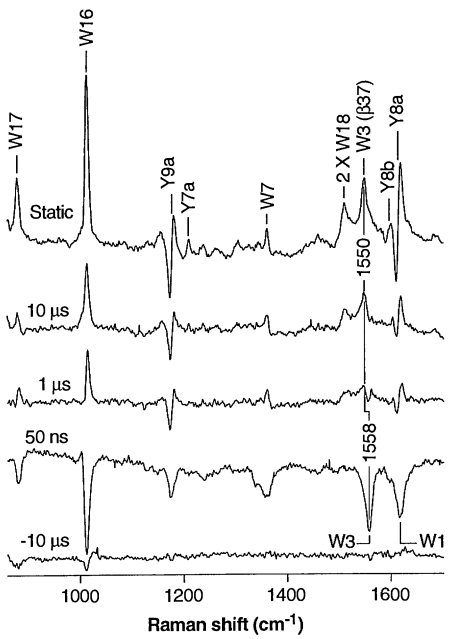

Fig. 1. Ultraviolet RR difference spectra obtained with excitation at 230 nm. The parent spectra were obtained by means of 135° backscattering from a stirred spinning quartz tube (*11*), with the use of a frequency-doubled XeCl excimer-pumped dye laser. Scattered light was collected with an *f*/1 Cassegrain mirror and coupled into a 1.25-m single spectrograph equipped with a grating (3600 grooves per millimeter) and into an intensified diode array detector. Subtraction of the parent spectra was carried out by zeroing the 985 cm^{-1} band of $NaClO_4$, present in the solutions at a concentration of 0.2 M. The top trace is the static difference spectrum between deoxyHb and HbCO; the remaining traces are pulse-probe difference spectra for HbCO, at the indicated delays with respect to a 419-nm photolysis pulse from a second excimer-pumped dye laser. The −10-μs trace (bottom) shows the level of subtraction artifacts.

K. R. Rodgers, Department of Chemistry, North Dakota State University, Fargo, ND 58105, USA.
T. G. Spiro, Department of Chemistry, Princeton University, Princeton, NJ 08544, USA.
*To whom correspondence should be addressed.

What is the nature of this tertiary change? A key is the position of the Trp W3 mode (*13*), near 1555 cm^{-1}. In the static and 10-μs difference spectra, a positive W3 band is seen at 1550 cm^{-1}, whereas in the 50-ns difference spectrum a negative W3 band is seen at a shifted frequency, 1558 cm^{-1}. The two frequencies are associated with different residues, the interfacial Trpβ37 at 1550 cm^{-1} and the interior Trpα14 and Trpβ15 at 1558 cm^{-1}, as has been established (*11*) with the aid of the mutant Hb Rothschild, which lacks Trpβ37. The frequency variation is associated with altered dihedral angles, $\chi^{2,1}$, about the bond connecting the indole ring with the β carbon atom (*11*, *20*). Thus, the 50-ns difference signals are associated with the interior Trp residues.

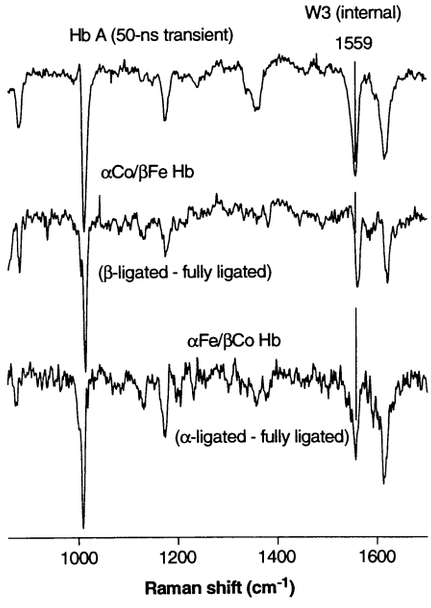

Fig. 2. Comparison of the 50-ns transient difference spectrum with static difference spectra of doubly ligated (CO adduct) minus fully ligated (O_2 adduct) of Co,Fe hybrid Hb, with Co substituted for Fe in the α chains (bottom) or in the β chains (middle). The hybrid Hb was prepared by a variation on the method of Ikeda-Saito *et al.* (*14*). Spectra were acquired as described in Fig. 1.

The Trpα14 and Trpβ15 residues are located on the A helices of the two subunits but form H bond interactions with the side chain hydroxyls of Thrα67 and Serβ72, located on the E helices and which line the distal sides of the heme binding pockets, as illustrated for the α chains in Fig. 3. The negative Trp peaks in the 50-ns difference spectrum, as well as in the Co,Fe difference spectra, indicate a loss in H bond strength of the indole NH, an effect known (*11*) to blue-shift the Trp excitation profile, resulting in diminution of the Raman intensity at 230 nm. Weakening of this H bond would be consistent with the E helix shifting its position toward the heme group and away from the A helix. The similarity of the two Co,Fe hybrid spectra indicate that both chains experience the same E helix motion. Because the negative peak at 1558 cm^{-1} is missing in the later pulse-probe difference spectra, we infer that the A-E helix separation is a transient phenomenon in native Hb. Comparison of the HbCO and deoxyHb crystal structures (*1*) reveals a displacement of the E helices toward the hemes, as indicated by the arrows in Fig. 3, but the Trpα14 and Trpβ15 H bonds are not much affected. We infer that the E helix motion initially weakens the H bonds, but they are restored on the microsecond time scale by a following motion of the A helices. The early E helix motion is concerted with departure of the CO from the binding pocket.

Previous discussions of the structural dynamics of the R-T transition have been dominated by consideration of the F helix that is proximal to the heme. Comparison of HbCO and deoxyHb crystal structures shows a ~1 Å lateral shift of the F helix, across the face of the heme (see arrows in Fig. 3), bringing the carboxyl side chains of Aspβ99 and Aspα94, located at the F-G helix corners, into position to form H bond contacts across the $\alpha_1\beta_2$ interface with the critical residues Tyrα42 and Trpβ37 (*1*). Gellin and Karplus (*21*) carried out molecular mechanics simulations along a minimum energy pathway between the static crystal structures and focused on the F helix and F-G corner as the "allosteric core" of Hb. Our results indicate, however, that there is a well-defined intermediate structure, involving E helix displacement, which is distinct from the equilibrium-ligated and deoxy structures. It is reasonable that the E and F helices form a dynamical unit, because they are linked at the E-F helix corner and they interact directly with the distal and proximal heme ligands, respectively.

These data are in fact consistent with early motion of the F, as well as the E, helix because the 50-ns transient species is characterized by a Tyr Y9a difference band (Figs. 1 and 2), as well as the Trp difference bands. A change in the environment of one or more Tyr residues is indicated. The most likely candidates are Tyrα140 and Tyrβ145, which are H-bonded to the carbonyl oxygens of Valα93 and Valβ98, respectively (*1*); these Val residues are located at the F-G corners.

We propose a model of the R-T reaction coordinate that starts with deligation of the heme and the simultaneous movement of the Fe atom toward the proximal His residue (*22*). These displacements, which can be induced photolytically on the subpicosecond time scale, induce strain in the E and F helices. Relief of this strain occurs by means of a concerted motion of the two helices in a "scissoring" motion (arrows in Fig. 3). The dissociated ligand departs from the heme pocket during this motion.

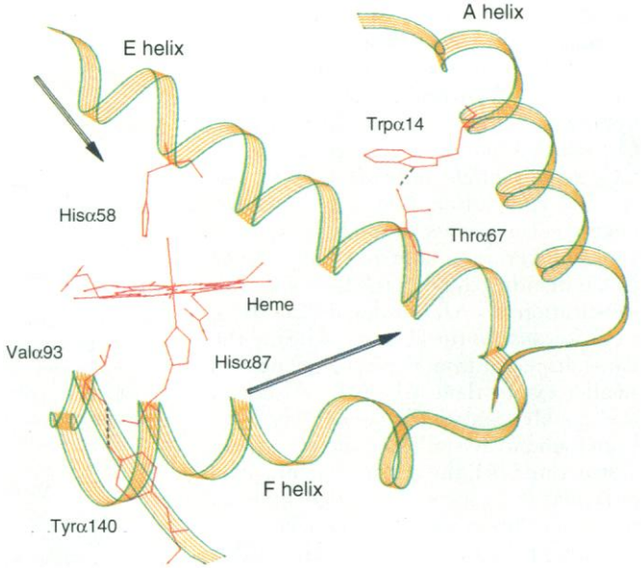

Fig. 3. Diagram of the helix arrangement around the heme pocket of the α chains of HbCO (*3*), showing the H bond between Trpα14 and Thrα67, which bridges the A and E helices, and the H bond between Valα93 and Tyrα140, which bridges the F-G corner and the COOH-terminus. The rearrangements are similar for the β chains, except that Trpβ15 and Serβ72 provide the A-E bridge, whereas Valβ98 and Tyrβ145 bridge the F-G corner and the COOH-terminus. The arrows indicate the direction and relative magnitudes of the helix displacements in deoxyHb, relative to HbCO (*1*). We propose that departure of the ligand from the heme pocket, subsequent to photodeligation, is associated with E helix motion toward the heme in concert with the indicated F helix motion, leading to the R-T rearrangement of the subunits.

REFERENCES AND NOTES

1. J. Baldwin and C. Chothia, *J. Mol. Biol.* **129**, 175 (1979).
2. G. Fermi and M. F. Perutz, *ibid.* **114**, 421 (1977); R. C. Ladner, E. G. Heidner, M. F. Perutz, *ibid.*, p. 385;

G. Fermi, M. F. Perutz, B. Shaanan, R. Fourme, *ibid.* **175**, 159 (1984).
3. J. L. Monod, J. Wyman, J. P. Changeux, *ibid.* **12**, 88 (1965).
4. M. F. Perutz, *Annu. Rev. Biochem.* **48**, 327 (1979); *Annu. Rev. Physiol.* **52**, 1 (1990).
5. J. J. Hopfield, R. G. Schulman, S. J. Ogawa, *J. Mol. Biol.* **61**, 425 (1971).
6. C. Sawicki and Q. H. Gibson, *J. Biol. Chem.* **251**, 1533 (1976); *ibid.* **254**, 4058 (1979).
7. G. J. Turner *et al.*, *Proteins Struct. Funct. Genet.* **14**, 333 (1992); G. K. Ackers, M. L. Doyle, D. Myers, M. A. Daugherty, *Science* **255**, 54 (1992); G. K. Ackers and J. H. Hazzard, *Trends Biochem. Sci.* **18**, 385 (1993).
8. J. L. Martin *et al.*, *Proc. Natl. Acad. Sci. U.S.A.* **80**, 173 (1983).
9. P. A. Anfinrud, C. Han, R. M. Hochstrasser, *ibid.* **86**, 8387 (1989).
10. J. Hofrichter, J. H. Sommer, E. R. Henry, W. A. Eaton, *ibid.* **80**, 2235 (1983).
11. K. R. Rodgers, C. Su, S. Subramaniam, T. G. Spiro, *J. Am. Chem. Soc.* **114**, 3697 (1992).
12. R. P. Rava and T. G. Spiro, *J. Phys. Chem.* **89**, 1856 (1985).
13. I. Harada and H. Takeuchi, in *Advances in Infrared and Raman Spectroscopy*, R. J. Clark and R. E. Hester, Eds. (Wiley, New York, 1986), vol. 13, chap. 3.
14. M. Ikeda-Saito, H. Yammamoto, T. Yonetani, *J. Biol. Chem.* **252**, 8639 (1977).
15. W. R. Scheidt, *J. Am. Chem. Soc.* **96**, 90 (1974); P. N. Dwyer, P. Madura, W. R. Scheidt, *ibid.*, p. 4815; R. G. Little and J. A. Ibers, *ibid.*, p. 4452.
16. B. Luisi and N. Shibayama, *J. Mol. Biol.* **206**, 723 (1989).
17. T. W. Scott *et al.*, *FEBS Lett.* **158**, 68 (1983).
18. J. M. Friedman, D. L. Rouseau, M. R. Ondrias, *Annu. Rev. Phys. Chem.* **96**, 471 (1982).
19. J. M. Friedman, T. W. Scott, R. A. Stepnoski, M. Ikeda-Saito, T. Yonetani, *J. Biol. Chem.* **258**, 10564 (1983).
20. T. Miura, H. Takeuchi, I. Harada, *J. Raman Spectrosc.* **20**, 667 (1989).
21. B. R. Gellin and M. Karplus, *J. Mol. Biol.* **171**, 489 (1983).
22. S. Dasgupta and T. G. Spiro, *Biochemistry* **25**, 5941 (1986).
23. We are grateful to J. Kincaid for the generous gift of Co,Fe hybrid Hb (NIH grant DK 35153). Supported by NIH grant GM 25158.

29 March 1994; accepted 26 July 1994

iaglu, a Gene from *Zea mays* Involved in Conjugation of Growth Hormone Indole-3-Acetic Acid

Jedrzej B. Szerszen, Krzysztof Szczyglowski, Robert S. Bandurski*

Plants contain most of the growth hormone indole-3-acetic acid (IAA) in conjugated forms believed to be inactive in promoting growth. The *iaglu* gene, which controls the first step in the biosynthesis of the IAA conjugates of *Zea mays*, encodes (uridine 5′-diphosphate-glucose:indol-3-ylacetyl)-β-D-glucosyl transferase. Protein synthesized by *Escherichia coli* that contained cloned 1-*O*-β-D-indol-3-ylacetyl-glucose complementary DNA (cDNA) was catalytically active. The predicted amino acid sequence of the cDNA was confirmed by amino-terminal sequencing of the purified enzyme. Homologous nucleotide sequences were found in all plants tested. The blockage or enhancement of *iaglu* expression may permit regulation of plant growth.

All plants examined thus far contain most of the growth hormone IAA in a conjugated, presumably inactive, form (*1–3*). Plants exhibit a growth response to applied free (unconjugated) IAA, and there is evidence that growth rate is a function of endogenous free IAA concentrations (*4*). These results indicate that growth is limited and controlled by the amount of free IAA. In contrast, the conjugates appear to serve functions other than growth promotion, such as IAA transport (*5*), protection of IAA against peroxidative attack (*6*), storage of IAA in seeds (*1*, *7*), and hormonal homeostasis (*4*). Both ester- and amide-linked IAA conjugates have been chemically characterized (*1*, *7*). Because of the rapidity of conjugate synthesis and hydrolysis in vivo, the function of IAA conjugates has been difficult to study (*2*). The ability to augment or impair IAA conjugation may lead to a better understanding of the physiology of hormone conjugation and to methods for control of plant growth. Therefore, we cloned the *iaglu* gene, which encodes the first step in the IAA conjugation pathway.

In corn (*Z. mays*), the pathway to the conjugates begins with the synthesis of 1-*O*-β-D-indol-3-ylacetyl-glucose (IAGlu) from uridine 5′-diphosphate-glucose (UDPG) and IAA, catalyzed by the enzyme IAGlu synthetase (UDPG:indol-3-ylacetyl)-β-D-glucosyl transferase (Fig. 1) (*8–10*).

$$\text{IAA} + \text{UDPG} \rightleftharpoons \text{IAGlu} + \text{UDP}$$

IAGlu is an acyl alkyl acetal, and its energetically unfavorable synthesis is followed by an energetically favorable transacylation of IAA from IAGlu to *myo*-inositol (Fig. 1) (*11*).

We used polyclonal antibody (*10*) purified by affinity chromatography to screen a cDNA expression library made from polyadenylated RNA extracted from W64A$^+$ inbred corn endosperm tissue collected 18 days after pollination. The library was constructed in a lambda ZAP II vector (Stratagene) (*12*). After amplification, it contained 4.2×10^8 plaque-forming units. Eight positive clones were identified from among 1.5×10^6 *E. coli* XL-1 Blue plaques containing isopropyl-β-D-thiogalactopyranoside (IPTG)–induced β-galactosidase fusion proteins with an immunoglobulin G secondary antibody conjugated to alkaline phosphatase (*13*). Positive cDNA inserts were excised with R408 helper phage and recircularized to generate subclones in the pBluescript SK$^-$ phagemid vector (*14*). Both strands of the largest insert [clone 3, 1731 base pairs (bp)] were sequenced (*15*). The sequenced clone carried an open reading frame of 1413 nucleotides that coded for 471 amino acids (Fig. 2) (*16*). The open reading frame was rich in G and C nucleotides (C + G = 69.7%).

A portion of the purified enzyme was chromatographed on a C_{18} 1-mm by 250-mm high-performance liquid chromatography (HPLC) column with 0.1% trifluoroacetic acid (TFA) as the solvent and a gradient of 90% v/v acetonitrile-water containing 0.85% TFA. Protein degradation occurs (*10*), but the single major peak was collected for amino acid sequencing of the NH_2-terminal end. The 18–amino acid sequence obtained was MAPXVLVVPF-

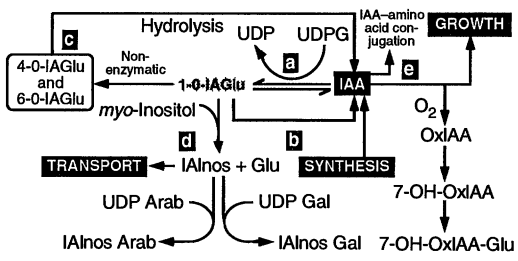

Fig. 1. Metabolic reactions that affect the concentration of IAA in *Z. mays*. (a) Reversible synthesis of 1-*O*-IAGlu from IAA and UDPG (*9*, *23*); (b) enzymatic hydrolysis of 1-*O*-IAGlu (*9*, *23*); (c) enzymatic hydrolysis of 4-*O*-, and 6-*O*-IAGlu produced by isomerization of 1-*O*-IAGlu (*23*, *24*); (d) transacylation of IAA from 1-*O*-IAGlu to form the transport ester, IAInos, and results in shifting the equilibrium toward esterified IAA (*7*, *8*, *11*); and (e) IAA may also be conjugated to amino acids (*1*, *7*).

J. B. Szerszen and R. S. Bandurski, Department of Botany and Plant Pathology, Michigan State University, East Lansing, MI 48824, USA.
K. Szczyglowski, Michigan State University–Department of Energy Plant Research Laboratory, Michigan State University, East Lansing, MI 48824, USA.
*To whom correspondence should be addressed.